Solar-Storm/Lunar Atmosphere Model (SSLAM): An Overview of the Effort and Description of the Driving Storm Environment

W. M. Farrell, J. S. Halekas, R. M. Killen, G. T. Delory, N. Gross, L. V. Bleacher, D. Krauss-Varben, D. Hurley, M. I. Zimmerman (others TBD).
122611

Abstract: On 29 April 1998, a coronal mass ejection (CME) was emitted from the Sun that had a significant impact on bodies located at 1 AU. The terrestrial magnetosphere did indeed become more electrically active during the storm passage but an obvious question is the effect of such a storm on an exposed rocky body like our Moon. The solar-storm/lunar atmosphere modeling effort (SSLAM) brings together surface interactions, exosphere, plasma, and surface charging models all run with a common driver – the solar storm and CME passage occurring from 1-4 May 1998. We present herein an expanded discussion on the solar driver during the 1-4 May 1998 period that included the passage of an intense coronal mass ejection (CME) that had > 10 times the solar wind density and had a compositional component of He^{++} that exceeded 20%. We also provide a very brief overview of the SSLAM system layout and overarching results. One primary result is that the CME driver plasma can greatly increase the exospheric content via sputtering , with total mass loss rates that approach 1 kg/s during the 2-day CME passage. By analogy, we suggest that CME-related sputtering increases might also be expected during a CME passage by a near-earth asteroid or at the Mars exobase, resulting in an enhanced loss of material.

I. Introduction

While the geo-effectiveness of solar storms and associated coronal mass ejections incident on the terrestrial magnetosphere are well-studied, the effect of such storms on exposed rocky bodies like the Moon has not been thoroughly examined. In 2008, a dedicated lunar science institute called the 'Dynamic Response of the Environment At the Moon (DREAM)' was

formed specifically to advance the understanding of the solar-lunar connection. One of the primary objectives of DREAM is to examine the response of the lunar exosphere, exo-ionosphere, and surface-plasma interactions during the passage of a solar storm/CME by the Moon; this using a combination of existing space weather data sets (from Wind, ACES, and Lunar Prospector spacecraft) as inputs to a set of interconnected models. This focused DREAM institute study has been called the solar storm-lunar atmosphere modeling (SSLAM) effort which commenced the summer of 2010 and resulting in a workshop in June 2011.

In the effort, institute team members attempted to advance the understanding of the radiation-plasma-surface interaction at the Moon during an extreme solar event. In this specific paper, we focus on the description of the prevailing, disturbed solar radiation and plasma environment flowing past the Moon between 1 to 4 May 1998; this information being used as the observational input to the SSLAM system. During this time, the Sun was very active, producing a series of CMEs that propagated past a Moon that was fully exposed and unprotected by the geomagnetic tail (~first quarter phase). The detailed lunar response that is predicted by SSLAM is presented by other papers in this special issue (Killen et al. [2011], Zimmerman et al. [2011], Stubbs et al. [2011], Hurley et al. [2011], Krauss-Varben et al. [2011]). In this work we emphasize the description of the solar driver.

The primary objective of SSLAM is to answer the question: How does energy and matter in a solar storm affect the exposed, unprotected lunar surface and its corresponding volatile, plasma, and dust environment. Specifically, how much mass is lost during a CME passage? How long do affects from the storm linger in the environment? Can spacecraft like Lunar Atmosphere and Dust Environment Explorer (LADEE), Acceleration, Reconnection, Turbulence and

Electrodynamics of the Moon's Interaction with the Sun (ARTEMIS), and Lunar Reconnaissance Orbiter (LRO) detect the effects of the storm?

Figure 1 illustrates the general aspects of the solar-lunar radiation and conductive connection. The Moon is immersed in a stream of solar energy and matter including solar wind ions and electrons, solar photonic radiation, and high energy charged particles. This solar energy has the ability to energize/activate the lunar surface to create desorbed atomic species that form the neutral exosphere, sputtered neutral and ion species, charged surfaces, and electrically-induced lofted dust. Micro-meteoroids in the inner heliosphere also continually bombard the surface creating secondary impact particulate ejecta (small dust), neutral vapor, and plasma impulses. In essence, the solar energy and heliospheric matter continually erodes the surface of the Moon (at a rate of 10's of g/s [Stern, 1999]) with the eroded products forming a dusty-plasma and neutral super-surface that extends 10-100 km about the Moon.

During a storm and CME passage, the solar drivers of photonic radiation, fast moving charged particles, and cooler dense plasma, all intensify greatly. Within a CME, the plasma densities increase, but the plasma also becomes He-rich, temporarily increasing the mass-flux incident at the Moon. It is thus reasonable to expect that the lofted dust layer, plasma interaction region, and neutral exosphere about the Moon might also all intensify in cadence. The exact nature and extent of this storm-time intensification is the motivation for the SSLAM effort.

The solar drivers associated with a solar storm include photonic UV and x-ray emission that propagates at the speed of light, this initiated at the time the CME is released from the Sun. High energy radiation from the CME (shock region) is also continuously emitted as the driver gas propagates at ~ 500-1000 km/s from the Sun to the Earth-Moon system. After a few days, the CME driver gas, itself, is finally incident at 1 AU. Compared to the nominal solar wind, the

density of the CME wind is increased by a factor of 10 and the fractional content of He^{++} in the CME wind can increase from the nominal 2% to over 20% [Skoug et al., 1999].

Figure 1 illustrates the response of the Moon to these drivers. Solar photonic radiation incident on the dayside creates thermal and photon desorption of surface volatiles [Stern, 1999] and releases photo-electrons that charge the surface with a net positive potential of a few volts [Manka, 1973] . Solar wind plasma protons at ~1 keV will sputter atoms from the surface regolith [Johnson, 1990]. Together, these processes create a neutral gas exosphere (i.e., a collisionless atmosphere) which is expected to intensify when the massive driver gas is incident on the surface. The plasma also creates surface charging: positive on the dayside due to the dominance of photoelectron emission and negative on the nightside as that surface balances plasma electron and ion flux level [Manka, 1973; Farrell et al.,2007]. There is also the formation of a trailing lunar wake region, where the body has absorbed solar wind ions leaving plasma densities as low as 0.1% of ambient solar wind levels [Halekas et al., 2005]. The polar regions have special environments and plasma inflow into permanently shadow craters may affect the retention of volatiles in these cold traps [Zimmerman et al., 2011a]

The general evolution of a solar storm/CME release has the following stages : 1) In association with the commencement of a CME, a solar flare emits intense x-rays, EUV, radio emission, and high energy charged particles from a process called magnetic reconnection of the solar magnetic field. The rearrangement of the solar magnetic field from reconnection converts magnetic energy into energetic particle energy. Some of these high energy particles are directed back toward the surface resulting in the x-ray emission . 2) As the CME propagates outward at a speed faster than the Alfven wave speed in the interplanetary medium, a collisionless shock forms that also accelerates particles to high energies to form a solar energetic particle (SEP)

event [Reames, 1990; Gopalswamy et al., 2002]. If the CME and shock are directed Earthward, they will take approximately 2-4 days to reach 1 AU, and during this interval the IP shock emits SEP electrons and ions, and will radiate radio emission. 3) After propagating in the interplanetary medium, the shock will pass by the Earth-Moon system, and this passage has a clear signature in the plasma character as an abrupt increase in magnetic field strength and plasma density that are consistent with conditions across an magneto-hydrodynamic discontinuity [Gurnett and Bhattacharjee, 2005]. For ~10s of hours, the observation point is then immersed in a post-shock warm plasma (often called the 'sheath' but we will refer to it as 'post-shocked plasma) where the plasma temperature has increased to 300000-500000K (30-50 eV). The plasma flow velocity will also increase after crossing the interplantery shock, which may initially seem counter-intuitive. However, in the frame of reference of the shock (moving outward at a speed faster than the upstream solar wind), the flow now has a sub-Alfvenic velocity. 4) A magneto-hydrodynamic discontinuity passes by the Moon, marking the transition of warm post-shocked plasma to cold plasma that is associated with driver gas of the CME. In this region, the magnetic field will display a characteristic twist in association with being in an MHD force-free equilibrium. Within this region, the driver gas densities can be a factor of 10-15 times the ambient solar wind levels and He^{++} concentrations will increase by 10 times over nominal solar wind levels (to become > 20% of the ambient ion concentration) [Skoug et al., 1999]. As we describe in section V, such heavy ions can be a sputtering source.

The presentation herein will describe the SSLAM system (Section II), describe in detail an ideal CME event for focused storm-lunar interaction study on 1-4 May 1998 (Section III), present very unusual surface charging observations provide by Lunar Prospector during this period (Section IV), give an short overview of the resulting modeling effort (Section V), and

then provide conclusions on the effort, including the analog at near-Earth asteroids and Mars exobase. More detailed reports on the effect of the storm are found in Killen et al. [2011], Zimmerman et al. [2011], Stubbs et al. [2011], Hurley et al. [2011], Farrell et al. [2011], and Krauss-Varben et al. [2011].

II. Solar Storm-Lunar Atmosphere Modeling System

Figure 2 shows a block diagram of the cross-integrating SSLAM system. Individual blocks represent separate codes (or sets of interconnected codes); each run on separate platforms and managed by a model curator (usually the model/code developer). The connecting lines show the flow of model data products between the codes. The set of models have a common input (1-4 May 1998 storm period) and exchange products in a specific sequence. As a consequence, the synthesized component-level models act quasi-coherently to form a system-level model that examines the solar-lunar connection in a way that has not been done previously.

In order to identify a common event trigger, an Extreme Event Selection Committee was formed that included a subset of team members from the DREAM science team. Their objective was to examine existing data sets and find a candidate solar storm/CME event with the criteria that: 1) the Moon be external to the terrestrial geomagnetic tail and magnetosheath, 2) there be a comprehensive set of upstream plasma and high energy particle observations obtained by solar wind monitoring spacecraft like Wind or Active Composition Explorer (ACE), 3) the event be rich in the multi-charged heavy ion He^{++}, 4) a lunar landed or orbital plasma sensing asset be available, 5) the event be well-studied by the space weather/terrestrial magnetosphere community.

During the Apollo era, there were landed plasma sensing assets like the Suprathermal Ion Detector Experiment (SIDE) that could correlate storm activity with surface charging. However, there was a lack of comprehensive solar wind and SEP observations during this period. Thus, CMEs from the modern period were considered better suited for study. An ideal period was found in 1998, at the start of the peak active period of solar cycle # 23. During this time, there was both a large number of upstream solar wind monitors and a plasma sensing system in lunar orbit: the magnetometer and electron reflectometer (MAG/ER) onboard the Lunar Prospector (LP) spacecraft. CMEs that were rich in He^{++} were found in early May, August and September of 1998.The May 1998 event was also part of the space weather SHINE campaign, and thus the focus of previous study. A such, the May 1-4 1998 event was selected as the driver for the study.

The observations from the upstream monitors Wind, ACE and Solar Heliophysics Observatory (SOHO) for 1-4 May 1998 form a common input database for a set of DREAM models. These models included a Monte Carlo lunar exosphere model [Hurley et al., 2000], global hybrid plasma simulation [Travnicek et al., 2005], surface charging and dust lofting system [Stubbs et al., 2006], polar crater plasma expansion [Farrell et al., 2010; Zimmerman et al., 2011a], polar crater resource calculation based on Johnson [1990], and roving object charging model [Jackson et al., 2011]. These existing components were modified and initially run in the sequence shown in Figure 2.

A key exchange was the transfer of sputters ion activity to the global hybrid plasma simulation. The output of the sputtering model was used as the input for the plasma simulation that is specifically designed to self-consistently trace the trajectory of the new Kaguya-discovered reflected ions [Saito et al., 2009] and sputtered ions during storm time conditions. Another key exchange was between the polar crater plasma expansion simulation [Zimmerman

et al, 2011a] to the object charging model [Jackson et al., 2011]. In this case, the local plasma environment existing at the bottom of a crater floor was used as an input into the electrical dissipation of a moving system being charged by contact electrification (tribo-charged).

III. The Disturbed Sun and Interplanetary Medium

The CME that arrived at the Earth-Moon system on 2 May 1998 was initiated in association with an M8 flare that occurred on 29 April at 16:30 UT. Figure 3 shows the GOES X-ray flux from 29 April to 7 May with the strong flare event clearly observed (shaded circle on the left-hand side of the figure). SEP electron flux was observed by instruments onboard the ACE spacecraft in association with the Earthward-directed CME, with flux levels gradually increasing by a factor of 10 to peak near 30 April. The peak in energetic electron flux activity then progressively decreased to return to nominal levels at the start of 2 May. The SEP ion flux levels showed a similar initial behavior, but after peaking remained at steady, high levels to more abruptly decrease near the start of 2 May. The SEP electron flux activity was considered moderate, especially in comparison to the X3 flare event on 6 May where subsequent SEP electron flux levels were observed to abruptly increase by over a factor of 250.

The low energy plasma associated with the 29 April flare arrived at the Earth-Moon system at the end of the day on 1 May. The time-averaged speed of the CME can be derived from the 1 AU distance traveled in about 53.5 hours, corresponding to an average speed of about 780 km/sec. Figure 4 shows the ACE plasma measurements from 1 to 5 May, including the plasma density, temperature, flow speed and absolute value of the magnetic field.

We divide the CME passage into 4 clearly-defined intervals: 1) Interval 1 is the period of time the Moon is immersed in nominal solar wind with a flow speed of about 450 km/sec (as

observed at the end of the interval). 2) Interval 2 is defined by the period the Moon is immersed in a post-shock plasma. At the start of interval 2, the interplanetary shock that forms at the front of the CME passes the Moon. In association with this passage, the plasma density abruptly increases by a factor of 4, the plasma temperature increase by a factor of ~ 3, and the flow speed also increases to 600 km/sec (to appear at a substantially slower speed of only 50 km/sec in the frame of reference of the faster CME). 3) Interval 3 defines the period the Moon is immersed in an 'early CME' cold plasma. At the start of Interval 3, the Moon passes through an MHD discontinuity to then become immersed in the CME driver plasma. This early CME plasma is moving near 650 km/sec, is substantially cooler than the post-shock plasma, and has a density comparable to the nominal solar wind value. We note that the measured velocity of 650 km/sec is below the overall average velocity value from the CME transit time, suggesting that the CME was ejected at substantially faster speeds and then progressively slowed as it moved towards Earth. 4) Interval 4 is defined as the period when the Moon becomes immersed in the very dense plasma in the later part of the CME. Admittedly, this boundary is somewhat arbitrary since there is not a clear MHD discontinuity associated with the passage. However, the character of the plasma in this late CME is distinctly different, having densities that are ~10 times that of the nominal solar wind. As indicated in Skoug et al., [1999], the concentration of heavy, multi-charged ions (He^{++}) substantially increased from a few percent in the nominal solar wind to have values lie between 20-30% in this late CME plasma. Thus, the plasma in this late CME period is not only denser, but also contains higher relative proportions of heavy, multi-charged ions. Table 1 captures the key plasma parameters of the 4 intervals. Many of the SSLAM studies will present simulation runs from each interval as separate slices, since some models cannot be run over the entire 4 day period.

A close inspection of Figure 3 reveals that in the middle of the passage of the CME driver gas, at 13:13 UT on 2 May, the Sun once again released a CME and flare-related energetic particles. While the CME would not arrive until after 3 May, the energetic electrons moving at relativistic speeds arrived at the Moon in association with the X1 flare event. Figure 5 shows the arrival of the SEP events in the collated WIND, SOHO and ACE high energy particle measurements [Halekas et al., 2009]. Note that the tan lines are indicative of the highest energy particles (4.4 MeV for electrons, and 33 MeV for ions) and these show a distinct and abrupt increase in association with the flare event. Some SSLAM studies incorporated this anomalous SEP event into their models to understand the effect such radiation might have on surface charging [Stubbs et al., 2011] and the plasma sheath [Farrell et al., 2011].

IV. Lunar Prospector Observations

The Lunar Prospector (LP) spacecraft provided a birds-eye view of the interaction of solar storms with the lunar environment, from its orbit at an altitude of ~100 km in 1998. LP had plasma instrumentation consisting of the Electron Reflectometer (ER) and Magnetometer (MAG) instruments. The ER was a top-hat electrostatic analyzer that measured full 3-D electron distribution functions. During the time period considered in this study, the ER energy sweep covered energies from 38 eV-17 keV. The MAG, meanwhile, was a 3-axis fluxgate magnetometer, providing observations of magnetic field vectors at 9 Hz. We also use data collated from Wind, SOHO, and ACE [Muller-Mellin *et al.*, 1995; von Rosenvinge et al., 1995; Gold *et al.*, 1998; Stone *et al.*, 1998] to characterize the energetic fluxes, as described in Halekas et al. [2009], like that shown in Figure 5.

By a lucky happenstance, the LP ER serendipitously proved capable of measuring surface negative electrostatic potentials, by inferring the potential drop using the energy dependence of the electron loss cone, and the energy of secondary and/or photoelectrons accelerated up to the spacecraft from a negatively charged surface. This technique was applied in an approximate fashion to both quiet time and solar energetic particle events [Halekas et al., 2007], and then later refined to include approximate corrections for spacecraft charging, as described in detail in Halekas et al. [2008] and Halekas et al. [2009].

The solar storms in May 1998 have been studied in detail by numerous authors [Burlaga et al., 2001; Farrugia et al., 2002; Torsti et al., 2004]. For our purposes, it is sufficient to know that a CME shock passed the Moon late on May 1st, followed by a magnetic cloud filled with cold plasma, with high fractions of heavy ions. As this dense plasma propagated through the solar system, a solar energetic particle event injected very energetic charged particles into the cloud structure. These events had a significant impact on the lunar environment, as shown in Fig. 6.

Panel b and c of Figure 6 shows an energy spectrogram for electrons, focusing on those electrons that are propagating up and down a magnetically-connected field line to the Moon. The consistent patches of red in the spectrogram are associated with locally generated photo-electrons, and thus indicate times when LP is in direct sunlight. However, between those times, the spacecraft is in shadow and connected to the nightside lunar surface, as indicated in panel e which shows large solar zenith angles at these times. Since the nightside surface is generally charged negative, beams of secondary electrons are ejected from the surface at energies near the local lunar surface potential. As such, these electron beams allow the remotely flying LP spacecraft to directly infer the surface potential. This potential derived from the surface-

accelerated secondary electron beams is shown in panel (d) which has been quantitatively determined using previously developed procedures [Halekas et al., 2008, 2009].

The derived lunar surface potential in panel (d) follow a clear trend with surface solar zenith angle, with most large negative potentials observed on the night side, and the largest potentials seen in the central wake. The reason for this dependence is clear; low energy plasma does not easily enter the wake at low altitudes, while higher energy particles have large gyroradii, allowing them to easily penetrate the wake. Therefore, energetic particles dominate in the central wake, allowing the surface to charge to large negative values.

Though the elevated fluxes of energetic electrons during this time period clearly have a significant affect on the magnitude of the surface charging, it is also apparent that they do not alone control the surface potential, since we observe elevated levels of charging even before the largest energetic particle injection at ~14:00 on May 2nd. Indeed, nightside surface potentials increase significantly soon after the passage of the shock (the large magnetic field amplification at ~22:00 on May 1st). The very low temperature plasma in the magnetic cloud provides a likely explanation for this elevation in charging. First, since the low temperature of the plasma implies that the thermal surface charging currents go down, any energetic particles present have a commensurately larger effect on surface charging during the magnetic cloud's passage. In addition, the secondary emission from the surface decreases significantly when the plasma temperature is very low, removing a factor that tends to mitigate large negative surface charging at other times. Therefore, the conditions during the passage of the cold CME plasma strongly favor the development of large surface potentials, and the subsequent injection of energetic particles enhances things even farther.

Though not the main focus of this paper, the dayside effects seen by LP are also of note (in panel e, where the SZA is below 90°). Fig. 6 shows the presence of highly variable "spiky" upward-going electron fluxes during this time period, together with unusually high levels of magnetic field fluctuations. The upward-going electron fluxes most likely indicate reflection from crustal magnetic fields on the surface, with some amplification of upward-going fluxes due to the effects of reflection from an obstacle in motion with respect to the plasma frame [Halekas et al., 2011]. These upward-going electrons most likely drive the high levels of magnetic field fluctuations, and can even affect the upstream plasma, thermalizing and diffusing the highly anisotropic fluxes incident on the Moon during the SEP injection, as described by Halekas et al. [2010].

V. Descriptive Overview of SSLAM Results

The SSLAM effort commenced in mid-year 2010. As indicated in Figure 2, specialized teams were formed to address the CME effects on the exosphere, surface charging, plasma interactions, and the polar environment. Model outputs were discussed, refined, and exchanged between the model curators. This activity continued to June of 2011when a lunar extreme workshop was held to examine model results and to form conclusions. The workshop also included participation from 10 high school students and two teachers from local Baltimore/Washington high schools as part of the institute's education effort. Prior to the workshop the student participated in a 16-week custom-designed course on the solar-lunar connection (see http://ssed.gsfc.nasa.gov/dream/DREAM/syllabus1.html). We review some of the topics and key results below, identifying the a subset of SSLAM paper that described the effects in greater detail.

Killen et al. [2011] found that the sputtering flux for neutral and ion species increases by many factors of 10 within the He^{++} -rich driver plasma of a CME as compared to nominal solar wind levels. This result can be understood by recognizing that, in general, sputtering yields vary with the linear energy transfer (dE/dx) of an ion within a given substrate, with $Y \sim (dE/dx)^n$, where n varies from 1 to 1.6 (see Eq. 3.27 of Johnson [1990] and Elphic et al., [1991]). This dE/dx varies directly with the mass of the incident ion, M (in units of proton mass) and is also proportional to the square of the charge of the incident ion , Z^2 [Johnson, 1990]. As such, one should expect yields for heavy, multi-charged ion species near 1 keV to vary approximately as $Y_s/Y_p \sim (M_s Z_s^2)^n$ where, Y_p is the proton yield, and Y_s is yield for the heavier species. Barghouty et al. [2011] recently provided detailed yield values from lunar-type regolith undergoing bombardment from heavy multi-charged ions including He^{++} like those expected in a solar wind-like plasma.

Motivated by this scaling effect of the sputtering yields, Killen et al. [2011] created a weighted yield appropriate for the CME driver plasma in 2-3 May 1998, and found that CME-sputtering becomes the dominant process in releasing material from the Moon with both volatile and refractory species have increased dayside source rates at 20-80 times higher than in the nominal solar wind. Hence species like Si, Fe, and Ti begin to populate the exosphere and escape the Moon. Over the course of the 2-day passage of the CME driver gas, there could be as much as 100 tons of mass eroded from the Moon via CME sputtering. While this loss is surprisingly large, we note that the CME itself also delivers about the same amount of material to the surface in the form of the driver-gas protons and heavy ions.

The results of the sputtered ion modeling [Killen et al, 2011] were then used as the input to a multi-dimensional hybrid plasma simulation [Krauss Varben et al. 2011] of the ion and

electron environment during the highly disturbed solar wind conditions in early May 1998. The results of this modeling, describe further in Krauss Varben et al. [2012] show that there is an enhanced CME storm time ion component of lunar origin that can propagate upstream to form a precursor layer during the CME passage.

Stubbs et al. [2012] reports that the surface charging at the equator and terminator regions is modified as the CME passes. Farrell et al., [2012] provides simulations showing that the dayside plasma sheath that traps photo-electrons in nominal solar wind conditions actually becomes less efficient in trapping during the passage of the CME, consistent with Stubbs et al. [2012] reduced dayside surface potential. Polar crater regions are also found to undergo very complex electrical interactions during the passage of a CME [Zimmerman et al, 2012]. Since the plasma expansion from the surface on to the crater floor scales with electron temperature, ions will more easily flow onto the crater floor while the Moon is immersed in the warm post-shock plasma. The large currents in the late part of the CME also find their way to the crater floor, where that can affect sputtering and the loss of volatiles. Ion sputtering losses affect the long term stability of volatiles that become trapped within these cold regions and these models provide a guide to quantify the loss of material from the crater floor. Using a modeling tool developed previously [Jackson et al., 2011], it was found that a tribocharged object inside the crater will easily dissipate accumulated charge when the warm sheath plasma passes the Moon, but will have greater relative difficulty dissipating negative charge in the early portion of the CME (Interval 3) with the substantially reduced ion influx to the crater floor.

Conclusions

We model the response of the lunar surface during the highly disturbed solar plasma and radiation environment at the Moon during the 1-4 May 1998 CME passage. Using the observational data sets from upstream plasma monitors (Wind,ACE, and SOHO) as common inputs/initial conditions, we considered the effect of the storm time solar energy and matter has on the surface charge, exosphere, within polar craters, and on the passing plasma flow. The driving solar energy is described in this work while the predicted responses are detailed in Killen et al. [2012], Zimmerman et al. [2012], Stubbs et al. [2012], Hurley et al. [2012], Krauss-Varben et al. [2012] and Farrell et al. [2012].

The key element to the SSLAM system is the integration of component models into one larger coherent system. This integration includes using a common triggering event and cross-exchanging model data products at key points in the process. The coordinated application of the component models creates a product greater than the sum of their parts – an overall system-level examination of the effect of a solar storm at the Moon.

One of the primary findings is that the neutral exosphere should become 'inflated' (i.e., denser and a larger scale heights) due to CME-sputtering involving the heavy ions in the driver gas. The 'bulked-up' exosphere could be observed by the Lunar Atmosphere and Dust Environment Explorer (LADEE) neutral mass spectrometer (NMS) and ultraviolet/visible spectrometer (UVS). Specifically, during a solar storm, one will expect a greater concentration of sputtered regolith-based species like Si and Fe beyond those values presented for nominal solar wind by Sarantos et al. [2011]. LADEE will fly in late 2013 near solar maximum and there is a reasonably high likelihood that a CME will pass the Moon during the 4-month period of spacecraft operation. As suggested by Sarantos et al. [2011], viewing of the fast sputtered component by the LADEE NMS may require the instrument to view at least partially in the nadir

direction (tilt downward relative to its nominal ram-facing direction), otherwise, the fast-ejected atoms may not easily enter the NMS system. Such a CME/Moon/LADEE event will provide ideal validation of the predictions presented in the SSLAM effort.

While the effect CME-sputtering exosphere enhancement and associated mass loss has been predicted for the Moon based on the SSLAM effort, the results should also apply to any exposed rocky body near 1 AU. Specifically, any Near Earth Asteroid (NEA) should also undergo a similar effect where the heavy, multi-charged ions in a CME sputter material off of the body. We also them might expect a similar inflation in the exosphere about these bodies during a solar storm. For a robotic precursor orbiter about a NEA, an onboard NMS or ion mass spectrometer (IMS) should then be able to perform an analysis of the surface material composition analysis by examining the species being sputtered from the surface. Neutral and secondary ion mass spectrometer are common lab methods for deriving atomic composition, and we are suggesting that solar storms provide the necessary driver plasma to perform a similar technique on a larger scale at NEAs.

The results from SSLAM also can be applied to gain a further understanding of atmospheric loss at the Martian exobase. It may not seem intrinsically obvious that the results from a solid can be applied at the collisional-collisionless boundary of a gas, but sputtering at 1 keV is dominated by momentum transfer, and thus is only dependent upon the density of scattering sites (i.e., nuclei) in a material [Johnson, 1990]. Thus, length scales are longer, but sputtering/atomic release by external plasma interaction at the exobase will occur in an analogous way as a solid. Chassefiere and Leblanc [2004] indicate that sputtering is one of ~4 competing mechanisms capable of atmospheric loss at Mars, and suggest sputtering was the dominant loss process > 1 Gya. Nominal loss rates are at $\sim 10^{24}$ oxygen atoms lost per second or

about 30 g per second. However, applying the SSLAM results, we should suggest that during a CME passage, the loss rates from sputtering could increase significantly (by factors of many 10's), temporarily making exobase CME-sputtering the dominant loss process in storm-time conditions. The Mars Atmosphere & Volatile Evolution (MAVEN) spacecraft will be launched in late 2013, in the solar maximum period and might detect enhanced sputtering effects from CME interactions with the planetary exobase.

An interesting corollary question is that if a CME releases ~50 times more Si and Fe from the lunar surface, where does the associated oxygen go? The Si and Fe in the lunar regolith is in the form of oxides, and sputtering should release copious amounts of O as well. However, an O exosphere about the Moon has not been directly measured [Stern, 1999]. The surface may require the bombardment by an He^{++} rich plasma like that found in a CME to release amounts of O large enough for confident UV detection by LADEE. Also, in our SSLAM determination of sputtering loss rates [Killen et al., 2011], O was not included since its post-release pathway is not well understood. Thus, the substantial CME-related mass loss described by Killen et al. [2011] does not include the potential loss of another key component, simply because its unclear what happens to this highly-reactive atom. LADEE thus may help solve this 'mystery of O' that was entertained during the SSLAM analysis.

We found that the passing CME did indeed affect the environment of the Moon at the macroscopic scale, creating an enhanced sputtered neutral and ion exospheric region, intense surface charging, and anomalous plasma inflows into polar and terminator craters (i.e., in topography where the plasma flow is primarily horizontal). Solar storms are seleno-effective, altering the near-surface lunar environment. Such environmental effects need to be considered in future exploration of the Moon or any airless, exposed rocky body.

Acknowledgements: This work was supported by the NASA Lunar Science Institute. We thank the ACE EPAM and SIS instrument teams, the Wind EPACT team, the SOHO COSTEP instrument team, and NASA's CDAWEB for providing energetic particle data.

References

Barghouty A. F., et al. (2011), Solar-wind protons and heavy ions sputtering of lunar surface materials, Nuclear Instruments and Methods in Physics Research B 269, 1310

Burlaga, L.F., R.M. Skoug, C.W. Smith, D.F. Webb, T.H. Zurbuchen, and A. Reinard (2001), Fast ejecta during the ascending phase of solar cycle 23: ACE observations, 1998-1999, *J. Geophys. Res., 106*, 20,957-20,977.

Chassefiere, E. and F. Leblanc (2004), Mars atmospheric escape and evolution: interaction with the solar wind, Planetary and Space Science 52 (2004) 1039–1058

Cintalla, M. J. (1992), Impact induced thermal effects in the lunar and Mercurian regoliths, J. Geophys, Res., 97, 947.

Crider, D. H., and R. R. Vondrak (2000), The solar wind as a possible source of the lunar polar hydrogen deposits, J. Geophys. Res., 105, 26773.

Elphic, R. C., et al. (1991), Lunar surface composition and solar wind induced secondary ion mass spectrometry, Geophys. Res. Lett., 18, 2165.

Farrell, W. M., T. J. Stubbs, R. R. Vondrak, G. T. Delory, and J. S. Halekas (2007), Complex electric fields near the lunar terminator: The nearsurface wake and accelerated dust, Geophys. Res. Lett., 34, L14201, doi:10.1029/ 2007GL029312.

Farrell, W. M., T. J. Stubbs, J. S. Halekas, R. M. Killen, G. T. Delory, M. R. Collier, and R. R. Vondrak (2010), Anticipated electrical environment within permanently shadowed lunar craters, J. Geophys. Res., 115, E03004, doi:10.1029/2009JE003464.

Farrugia, C.J., M. Popecki, E. Mobius, *et al.* (2002), Wind and ACE observations during the great flow of 1-4 May 1998: Relation to solar activity and implications for the magnetosphere, *J. Geophys. Res.*, 107, 1240, doi:10.1029/2001JA0001888, 2002.

Gold, R.E., S.M. Krimigis, S.E. Hawkins III, D.K. Haggerty, D.A. Lohr, E. Fiore, T.P. Armstrong, G. Holland, and L.J. Lanzerotti (1998), Electron, Proton, and Alpha Monitor on the Advanced Composition Explorer, *Space Sci. Rev., 86,* 541-562.

Halekas, J. S., S. D. Bale, D. L. Mitchell, and R. P. Lin (2005), Electrons and magnetic fields in the lunar plasma wake, J. Geophys. Res., 110, A07222, doi:10.1029/2004JA010991.

Halekas, J.S., G.T. Delory, D.A. Brain, R.P. Lin, M.O. Fillingim, C.O. Lee, R.A. Mewaldt, T.J. Stubbs, W.M. Farrell, and M.K. Hudson (2007), Extreme lunar surface charging during solar energetic particle events, *Geophys. Res. Lett., 34,* L02111, doi:10.1029/2006GL028517.

Halekas, J.S., G.T. Delory, R.P. Lin, T.J. Stubbs, and W.M. Farrell (2008), Lunar Prospector observations of the electrostatic potential of the lunar surface and its response to incident currents, *J. Geophys. Res., 113,* A09102, doi:10.1029/2008JA013194.

Halekas, J.S., G.T. Delory, R.P. Lin, T.J. Stubbs, W.M. Farrell (2009), Lunar surface charging during solar energetic particle events: Measurement and prediction, *J. Geophys. Res., 114,* A05110, doi:10.1029/2009JA014113.

Halekas, J.S., Y. Saito, G.T. Delory, W.M. Farrell (2010), New views of the lunar plasma environment, Planet. Space Sci., in press, doi:10.1016/j.pss.2010.08.011.

Halekas, J.S., A. Poppe, G.T. Delory, W.M. Farrell, M. Horányi (2011), Solar wind electron interaction with the dayside lunar surface and crustal magnetic fields: Evidence for precursor effects, *Earth Planets Space*, in press.

Jackson, T. L, et al. (2011), Discharging of roving objects in the lunar polar regions, J. Spacecraft Rockets, 48, 700

Johnson, R. E. (1990), Energetic Charged Particle Interactions With Atmospheres and Surface, Spinger, New York.

Manka, R. H. (1973), Plasma and potential at the lunar surface, in Photon and Particle Interactions With Surfaces in Space, edited by R. J. L. Grard, pp. 347-361, Reidel, Dordrecht, Netherlands

Muller-Mellin, R., H. Kunow, V. Fleissner, *et al.* (1995), COSTEP – Comprehensive Suprathermal and Energetic Particle Analyser, *Sol. Phys., 162*, 483-504.

Saito, Y., et al. (2008), Solar wind proton reflection at the lunar surface: Low energy ion measurement by MAP-PACE onboard SELENE (KAGUYA), Geophys. Res. Lett., 35, L24205, doi:10.1029/ 2008GL036077.

Skoug, R. M., et al. (1999), A prolonged He+ enhancement within a coronal mass ejection in the solar wind, Geophys. Res. Lett., 26, 161.

Stern, S. A.(1999), The lunar atmosphere: history, status, current problems and context, Rev. Geophys., 37, 453.

Stone, E.C., C.M.S. Cohen, W.R. Cook, et al. (1998), The Solar Isotope Spectrometer for the Advanced Composition Explorer, *Space Sci. Rev., 86*, 357-408.

Stubbs, T. J., R. R. Vondrak, and W. M. Farrell (2006), A dynamic fountain model for lunar dust, Adv. Space Res., 37, 59, doi:10.1016/j.asr.2005.04.048

Torsti, J., E. Riihonen, and L. Kocharov (2004), The 1998 May 2-3 magnetic cloud: An interplanetary "highway" for solar energetic particles observed with SOHO/ERNE, *Astrophys. Journ.*, *600*, L83-L86.

Trávníček, P., P. Hellinger, D. Schriver, and S. D. Bale (2005), Structure of the lunar wake: Two-dimensional global hybrid simulations, *Geophys. Res. Lett.*, 32, L06102, doi:10.1029/2004GL022243

von Rosenvinge, T.T., L.M. Barbier, J. Karsch, et al. (1995), The energetic particles: Acceleration, composition, and transport (EPACT) investigation on the Wind spacecraft, *Space Sci. Rev.*, *71*, 155-206.

Zimmerman, M. I., W. M. Farrell, T. J. Stubbs, J. S. Halekas, and T. L. Jackson (2011a), Solar wind access to lunar polar craters: Feedback between surface charging and plasma expansion, Geophys. Res. Lett., 38, L19202, doi:10.1029/2011GL048880.

Killen et al.
Zimmerman et al.,
Stubbs et al.,
Hurley et al.
Krauss-Varben et al.,
Farrell et al

Sarantos 2011

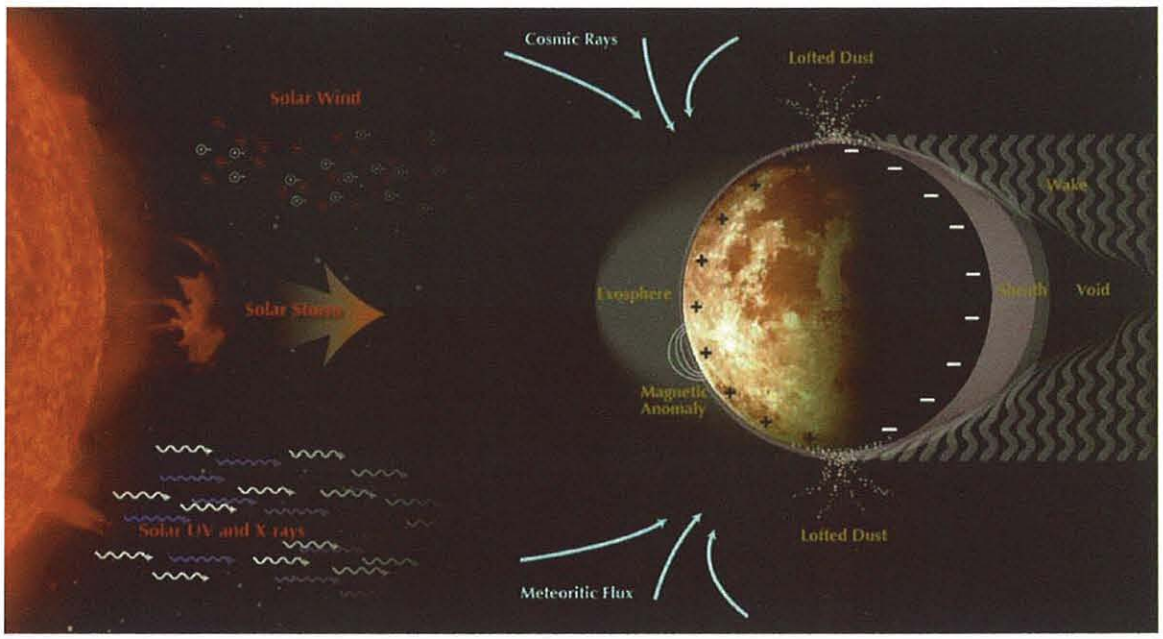

Figure 1- An illustration of the dynamic lunar environment driven by solar radiation and plasma. This environment responds to the energy in a solar storm, including that in a CME.

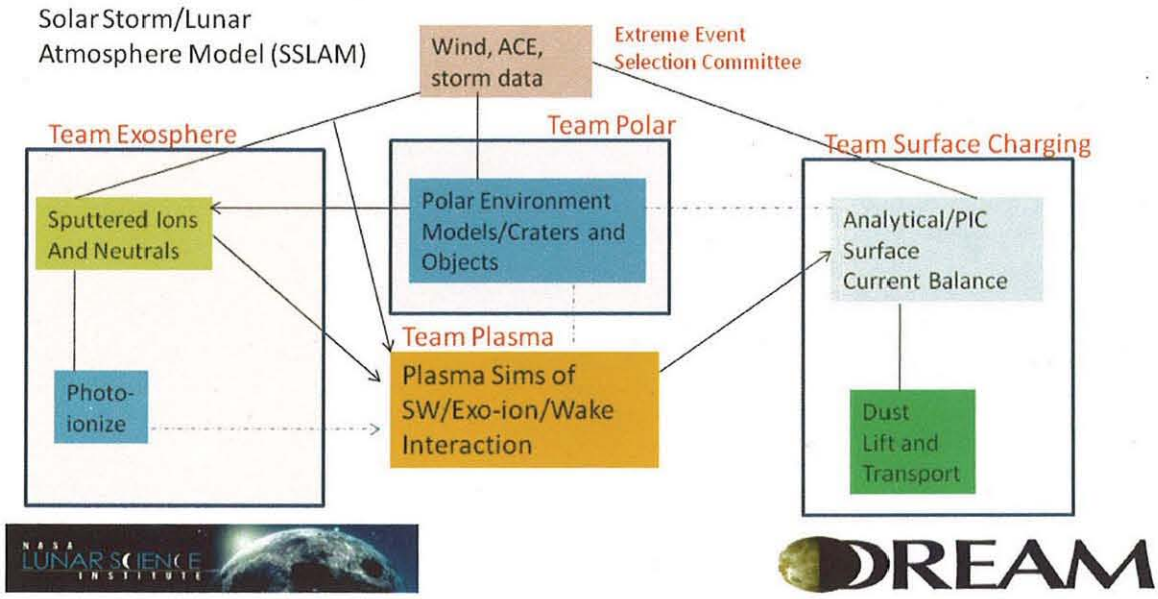

Figure 2- A block diagram of the Solar Storm/Lunar Atmosphere Modeling (SSLAM) effort.

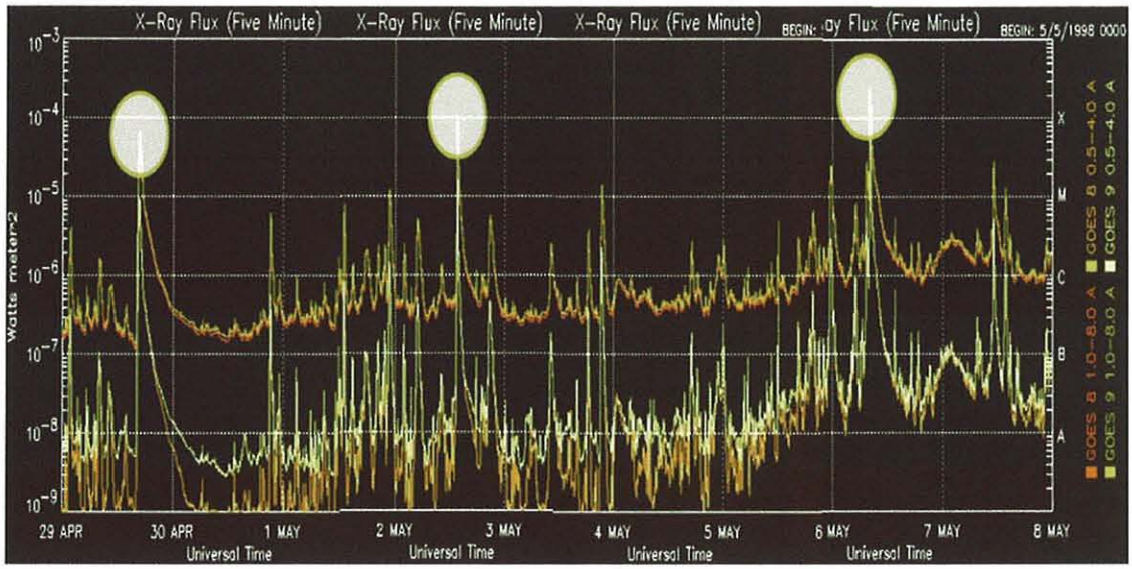

Figure 3- GOES x-ray flux indicating flare activity in early May 1998.

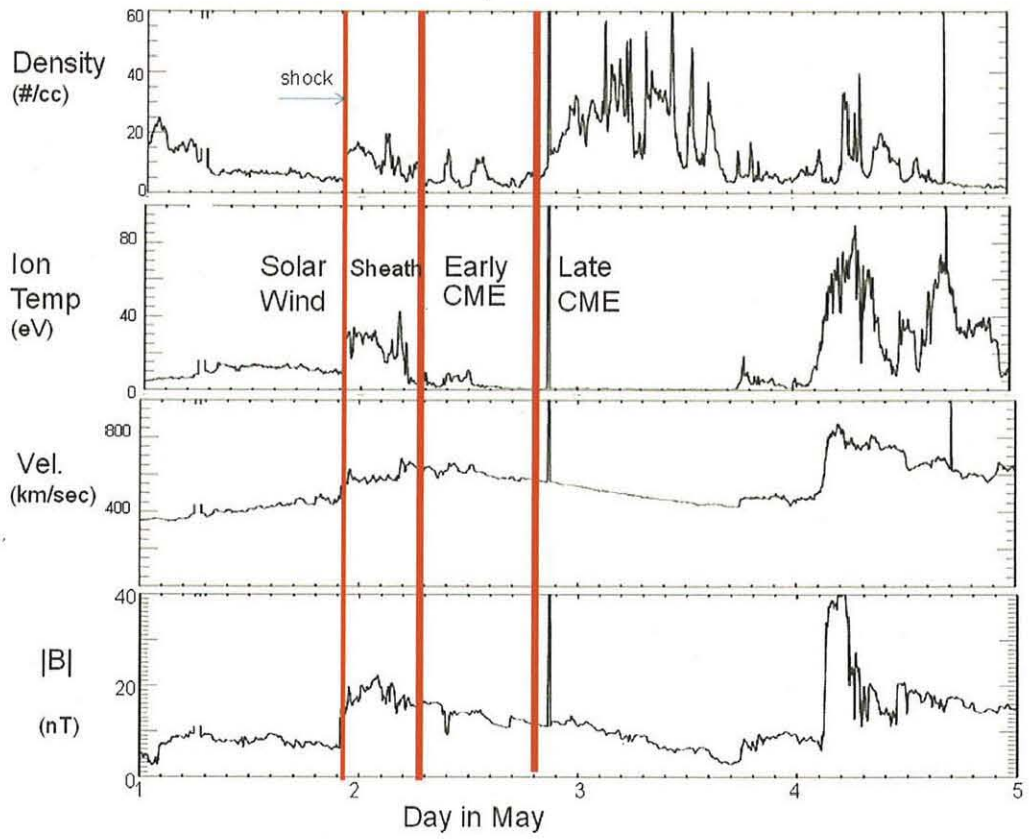

Figure 4 – The properties of the plasma during the CME passage by the Earth-Moon system in 2-3 May 1998 from the ACE spacecraft. Shown in sequence are the density, temperature, flow velocity, and magnetic field strength of the passing plasma.

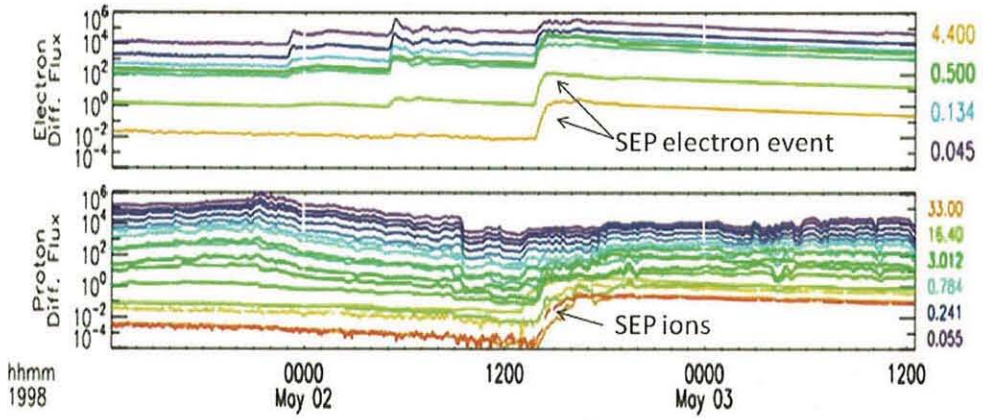

Figure 5- The energetic electrons and ions as observed by the upstream WIND-ACE-SOHO monitors during early May 1998. Note the passage of an SEP event near mid-day 2 May.

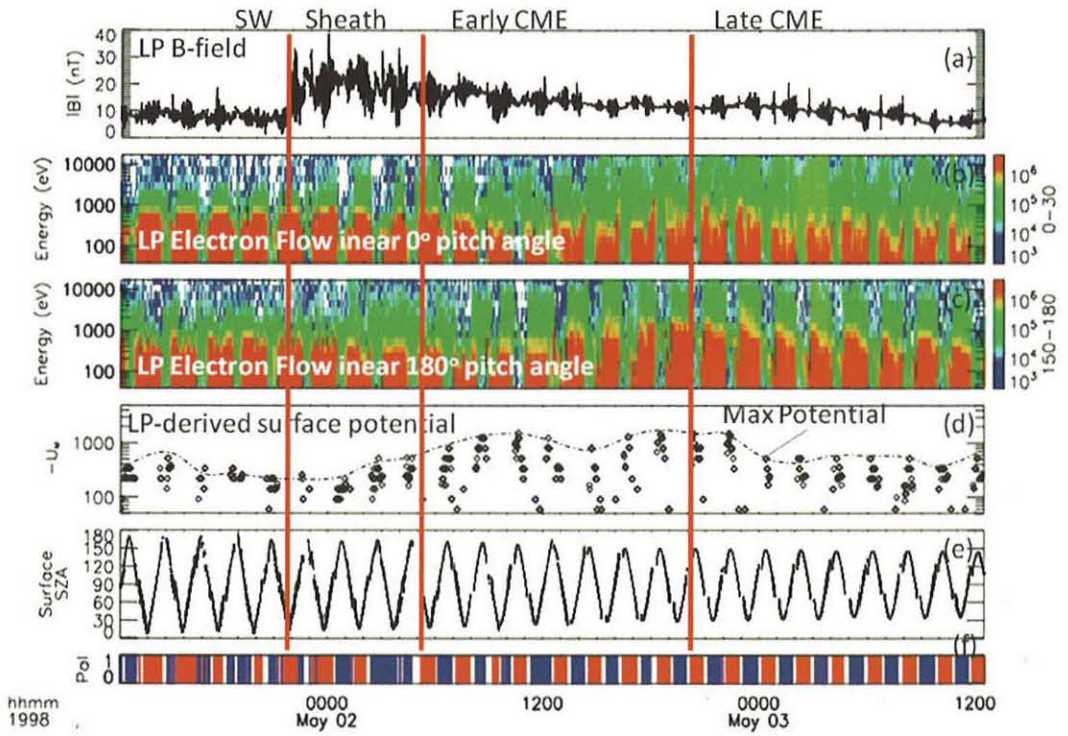

Figure 6- The Lunar Prospector MAG/ER observations of magnetic field and electron activity in early May 1998. In sequence, the top panel shows the strength of the magnetic field, the next two panels are electron energy vs time spectrograms for the magnetic field-aligned electrons (those electrons within 30° of the magnetic field). The strong red regions are local photo-electrons indicating the periods when the spacecraft is located in sunlight. The fourth panel is the lunar nightside surface potential derived from secondary electron beams. Note that these beam observations only occur when the solar zenith angle in the fifth panel is > 180°. The color bar at the bottom indicates polarity of the magnetic field line connected to the surface (red = plus, blue = minus).

Interval	#1	#2	#3	#4
Parameter	1998-05-01/16:00 Solar wind	1998-05-01/22:00 Shock/sheath	1998-05-02/06:30 Early CME	1998-05-02/19:30 Late CME
N_e (cm-3)	5	20	3	> 50
T_p (^{o}K)	1×10^5	~5×10^5	8×10^4	3×10^4
V_{sw} (km/sec)	450	600	650	500
He^{++}/H^+	0.02	0.001	0.1	0.2-0.3

Table 1 – The plasma parameters during the four intervals defining the 2 May 1998 CME passage. Interval #4 is most interesting when the solar wind density increases by > 10 times but also has a high concentration of heavy, multi-charged ions [Skoug et al., 1999].